


Flexible regions govern promiscuous binding of IL-24 to receptors IL-20R1 and IL-22R1

Jiří Zahradník^{1,2}, Lucie Kolářová¹, Yoav Peleg², Petr Kolenko^{1,3}, Silvie Svidenská¹, Tatsiana Charnavets¹, Tamar Unger², Joel L. Sussman² and Bohdan Schneider¹ 

¹ Institute of Biotechnology of the Czech Academy of Sciences, BIOCEV, Vestec, Czech Republic

² Weizmann Institute of Science, Rehovot, Israel

³ Faculty of Nuclear Sciences and Physical Engineering, Czech Technical University in Prague, Prague, Czech Republic

Keywords

IL-24; interleukin 24; promiscuity of receptor binding; protein design; protein stability

Correspondence

B. Schneider, Institute of Biotechnology of the Czech Academy of Sciences, BIOCEV, CZ-252 50 Vestec, Czech Republic
 Tel: +420 728 303 566

E-mail: bohdan.schneider@gmail.com
 Jiří Zahradník and Lucie Kolářová have contributed equally to the work.

(Received 8 March 2019, revised 5 May 2019, accepted 30 May 2019)

doi:10.1111/febs.14945

Interleukin 24 (IL-24) is a cytokine with the potential to be an effective treatment for autoimmune diseases and cancer. However, its instability and difficulties in its production have hampered detailed biological and biophysical studies. We approached the challenges of IL-24 production by using the PROSS algorithm to design more stable variants of IL-24. We used homology models built from the sequences and known structures of IL-20 and IL-19 and predicted and produced several extensively mutated IL-24 variants that were highly stable and produced in large yields; one of them was crystallized (IL-24B, PDB ID 6GG1; 3D Interactive at http://proteopedia.org/w/Journal:FEBS_Journal:1). The mutated variants, however, lost most of their binding capacity to the extracellular parts of cognate receptors. While the affinity to the receptor 2 (IL-20R2) was preserved, the variants lost affinity to IL-20R1 and IL-22R1 (shared receptors 1). Back engineering of the variants revealed that reintroduction of a single IL-24 wild-type residue (T198) to the patch interacting with receptors 1 restored 80% of the binding affinity and signaling capacity, accompanied by an acceptable drop in the protein stability by 9 °C. Multiple sequence alignment explains the stabilizing effect of the mutated residues in the IL-24 variants by their presence in the related and more stable cytokines IL-20 and IL-19. Our homology-based approach can enhance existing methods for protein engineering and represents a viable alternative to study and produce difficult proteins for which only *in silico* structural information is available, estimated as >40% of all important drug targets.

Introduction

Evolution optimizes proteins to function in living organisms, however, proteins used for research and applications often need to be stable under a wider range of conditions. A key function of a protein is binding to its proper partner(s), and avoiding inappropriate associations. The optimization of this process [1,2] and self-assembly into symmetric supramolecular complexes [3,4] often results in proteins that are marginally stable *in vivo* [5] and difficult to produce

in vitro, as is the case of many medically important proteins.

Low protein stability is characterized by low temperature denaturation, short half-life [6], low expression yields [7] and limited stability against denaturing agents [8]. Production of stable recombinant proteins therefore represents a substantial challenge. In recent years, methods of protein engineering have been undergoing a technological revolution enabled by the

Abbreviations

IL-10, interleukin 10; IL-19, interleukin 19; IL-20, interleukin 20; IL-24, interleukin 24.

growing number of sequenced genomes, experimentally determined biomolecular structures, and by deep mutational scanning procedures [9]. These technologies have enabled exploration of the vast space of protein properties, together with computational methods that have streamlined the selection of promising variants while avoiding predictions of false positives [5,10–13]. The synergy between bioinformatic analysis of a large volume of sequence data, together with experimental structures, has proven to be a powerful tool to overcome limitations in protein expression. Two such algorithms PROSS [14] and FireProt [15] that are already available on web servers, have made laborious, time-consuming, expert-requiring analysis of the sequence and structural data accessible to molecular biologists and protein chemists. These servers, as well as other approaches [16,17], combine force-field homology modeling by Rosetta [18] or FoldEX [19] with evolutionary consensus inferred from phylogeny to propose a large number of stabilizing mutations with a low rate of false positives.

We decided to apply these new protein engineering techniques to research of Interleukin 24 (IL-24), a member of Interleukin 10 family. The gene for interleukin 24 has been identified independently in fundamentally different biological contexts. Paul Fisher and coworkers described *IL-24* as a melanoma differentiation-associated gene-7 (MDA7) with an up-regulated expression in terminally differentiated human melanoma cells [20]. A few years later, a gene *c49a* was identified associated with wound repair [21], and at the same time, the gene named *mob-5* induced by *ras* oncogenes was identified in rat embryonic fibroblasts [22]. As it turned out later, all three genes represent human or rat orthologs of IL-24.

The great potential for medical applications of IL-24 goes well beyond its cytokine functions. Interest in this molecule has grown in connection to its potential anticancer activities. IL-24 being hailed as a ‘magic bullet’ and the ‘Holy Grail of immunotherapy’ [23], or ‘cancer’s Achilles heel’ [24]. However, other studies are at odds with the promises of IL-24’s anticancer activities and explain the observed phenomena differently [25,26]. In any case, the IL-24 is a fascinating molecule and its physiological and ‘supra-physiological’ properties cannot be ignored, however questionable or controversial it may seem.

The signaling of all IL-10 family members is mediated by the Janus Kinase/Signal Transducer and Activator of Transcription (JAK/STAT) pathway. IL-24 binds to receptor complexes and activates the STAT3 and STAT1 signaling [27,28]. It forms an IL-20 subfamily with IL-19, IL-20, IL-22 because all these

interleukins use the common class II cytokine receptor subunits and have similarities in biological functions [29]. IL-24 signals via two heterodimeric receptor complexes IL-22R1/IL-20R2 (IL-24 receptor complex, type II, Fig. 1) and IL-20R1/IL-20R2 (IL-20 receptor complex, type I). The IL-20 receptor complex is shared with IL-19 [30] and the IL-22 receptor is shared with IL-20 [27]. The structural reason for receptor sharing has been described thanks to known IL-20 ternary complex structure studies [31]. Receptor sharing and interleukin crosstalk are key mechanisms that the members of IL-10 family use to regulate its specific effects [32]. The affinities have not been known for IL-24 complexes, but the higher affinity for IL-20R2 is to be expected [30].

While the cells secreting IL-24 are hematopoietic, the target tissues include skin, lung, and reproductive organs [28]. This pattern corresponds to functions of the other IL-20 subfamily members which facilitate the communication between the immune system and epithelial cells, and modulate defense mechanisms, tissue repair processes at epithelial surfaces, and metabolic processes [29]. It is therefore not surprising that IL-24 is associated with multiple diseases, including the promotion and amplification of inflammatory responses during autoimmune and chronic inflammation [29], psoriasis-like skin inflammation [34], epidermal inflammation induced by stresses [35], inflammatory bowel disease [36,37], and also with host defense during bacterial infection [38].

To explore the IL-24 function, we used the PROSS server to design stable IL-24 variants to overcome aggregation and low yields of expression [39]. We applied the PROSS algorithm by using homology models instead of an experimental structure, as no

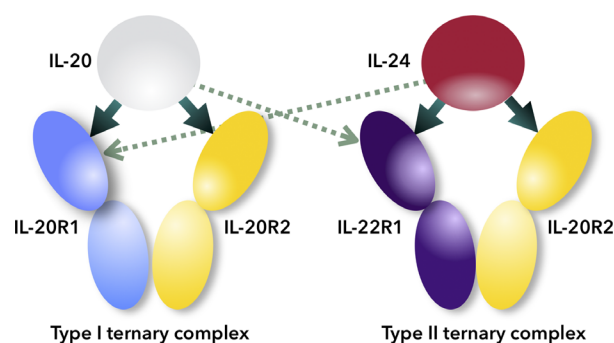


Fig. 1. Schema of promiscuous binding of IL-20 and IL-24 to signaling receptors IL-20R1 and IL-22R1 [33]. Arrows indicate binding between cytokines and their receptors; thick arrows show preferential binding, dashed ones alternative binding to the promiscuous receptors.

IL-24 3D structure was available at the time the study was initiated. Considering the fact that homology models are estimated to cover up to 70% of the human proteome, much more than available experimentally [40], this is a tempting and (as our results show) a viable strategy.

We demonstrated that a subset of all the suggested PROSS-designed variants resulted in high levels of soluble expression of IL-24 in *Escherichia coli*. This enabled us to pursue the structure and function of the designed IL-24 variants and to determine an apo 3D structure of one of them (PDB 6GG1). The analysis of the computationally designed structure pointed to the key residues controlling the protein stability. The most stable PROSS-designed protein (designated IL-24P7) showed very poor binding to its natural receptors. Extensive characterization of the structure and binding characteristics allowed us to link the increased stability primarily to changes at the binding interfaces to the IL-24 signaling receptors, IL-20R1 or IL-22R1, while the IL-24 receptor interface with IL-20R2 remained virtually unchanged. The binding to IL-20R1 or IL-22R1 was restored by reverting a single residue (T198R) of the PROSS-designed changes back to the wild-type sequence, but this resulted in a less stable protein.

Results and Discussion

IL-24 wild-type expression attempts

In order to obtain a viable process for IL-24 production, we put a lot of effort into conventional production systems based on *E. coli* pET plasmid systems, insect Schneider S2 cells, human HEK293 cells (Table 1), and to published protocols based on thioredoxin [41] or refolding of inclusion bodies [42–45]. None of these constructs showed a sufficient level of expression and/or protein quality that was satisfactory for further biophysical or structural studies. The experimental approach to increase the expression and solubility by the yeast surface display [46] was not possible due to the very limited expression of our construct. We therefore decided to overcome this challenge by *in silico* design of stabilized IL-24 variants.

Design of stabilized IL-24 variants

We used the PROSS algorithm to design potentially more stable variants of IL-24 for structural and biophysical characterization. So far, PROSS requires known 3D structure for designing more stable variants. As there was no known 3D structure of IL-24 at

the time of initiation of the project, we generated homologous models based on the known structures of related cytokines IL-20 (PDB 4DOH) and IL-19 (PDB 1N1F) using available servers: Swiss-model [47], Modeler implemented in Chimera [48,49], and I-TASSER [50] (Fig. 1). These models were then employed in the automated PROSS server [14] as the 3D structure template. To increase the probability of introducing stabilizing mutations, we combined outputs from multiple template models and, in addition, we used the FireProt [15] protein stabilization server. The mutations that were suggested by multiple models and by both servers were preferred.

Based on the PROSS-suggested mutations, we prepared three different constructs with different numbers of mutations, designated IL-24P3, IL-24P5, and IL-24P7, and tested their expression by using the bdSUMO tag system [51,52] (Fig. 2, Table 2). The most mutated construct, with as many as 34 mutations (IL-24P7), demonstrated a significant increase in the soluble fraction in *E. coli* and a large overall yield $\sim 100 \text{ mg} \cdot \text{L}^{-1}$ (Table 2). Five of the 34 changes cannot be viewed as mutations because they represent natural variants known from the single nucleotide polymorphism database, dbSNP: A89V (rs770135680), V131L (rs3093446), D164E (rs747187073), R174Q (rs539103349).

The most stable IL-24 variants do not bind to signaling receptors 1

We measured the binding affinities of IL-24wt and IL-24P7 to the extracellular part of the cognate receptors (Table 2). While both variants showed similarly high binding affinities to the shared IL-20R2 receptor, the stabilized variants had low, or no measurable affinity to the signaling receptors IL-20R1 and IL-22R1. The inability of this protein variant to initialize the signaling cascade was also confirmed by a STAT3 dual-luciferase assay on HeLa cells. We therefore decided to inspect the PROSS-introduced mutations in detail to uncover how they influenced the affinity. The task became possible due to the recently published crystal structure of the ternary complex of IL-24 fused to IL-22R1, and coexpressed with IL-20R2, PDB ID 6DF3 [53]. The IL-24 solved crystal structure has four mutations relative to the canonical UniProt ID Q13007 sequence, three removed glycosylation sites, and a naturally occurring variation Y124H (dbSNP: rs1150258). It is tethered to the signaling receptor IL-22R1. We set out crystallization trials of the stable apo IL-24 variants that are mentioned in Table 2. Diffraction quality crystals were obtained only for the variant called IL-24B. It is an IL-24P7 variant with 30 mutations

Table 1. An overview of IL-24 expression attempts with different constructs and systems

Vectors	Insert/Gene	Construct	Organisms/strains tested for expression	Expression
pET26b	IL-24wt (52-206)	IL-24wt	<i>E. coli</i> BL21, Shuffle, Rosetta, AE, C41, C43	No (SDS/PAGE)
pBAD	IL-24wt (52-206)	IL-24wt	<i>E. coli</i> BL21, Shuffle, Rosetta, AE, C41, C43, DH5 α , XL-1	No (SDS/PAGE)
pET26b	IL-24wt (52-206)	IL-24-C-His	<i>E. coli</i> BL21, Shuffle, Rosetta, AE, C41, C43, LEMO	No (SDS/PAGE)
pET28b	IL-24wt (52-206)	IL-24-N-His	<i>E. coli</i> BL21, Shuffle, Rosetta, AE, C41, C43	No (His antibody)
pET28b	IL-24wt (1-206)	IL-24-full-C His	<i>E. coli</i> BL21, Shuffle, Rosetta, AE, C41, C43	No (His antibody)
pET26b	IL-24wt (52-206)	IL-24wt, c-his, N-his 2S-S	<i>E. coli</i> BL21, Shuffle, Rosetta, AE, C41, C43	No (SDS/PAGE)
pET26b	IL-24wt (52-206)	IL-24wt, c-his, N-his 3S-S	<i>E. coli</i> BL21, Shuffle, Rosetta, AE, C41, C43	No (SDS/PAGE)
pET32a	IL-24wt (52-206)	trxA-IL-24	<i>E. coli</i> BL21, Shuffle, Rosetta, AE, C41, C43	No, or very low; Published—PMID: 17292626
pET28b	IL-24wt (52-206)	MBP-IL-24	<i>E. coli</i> BL21	Low (SDS/PAGE)
pET28b	IL-24wt (52-206)	HALO-IL-24	<i>E. coli</i> BL21	Low (SDS/PAGE)
pET28b	IL-24wt (52-206)	IL-24 N MBP-SUMO	<i>E. coli</i> BL21	Low, obstacles with cleavage; Published—PMID: 25681151
pET32a	IL-24wt (52-206)	IL-24 N EspA	<i>E. coli</i> BL21	Low; Published—PMID: 20854850
pET22b	IL-24wt (52-206)	IL-24 C His	<i>E. coli</i> BL21	Very low; PMID: 18953678
pET26b	IL-24wt (52-206)	IL-24-Cys1;Cys2;Cys3	<i>E. coli</i> BL21, Shuffle, Rosetta, AE, C41, C43	No, or very low (SDS/PAGE)
pMTH (variant of pMT-BiP-V5-HisB)	IL-24wt (50-206)	IL-24-C-His	<i>Drosophila</i> S2 cells (BiP leader—secretion)	No secretion (Ni-nitrilotriacetic acid purification, small scale, 50 mL)
pMTH (variant of pMT-BiP-V5-HisB)	IL-24wt (51-206)	IL-24-C-His	<i>Drosophila</i> S2 cells (BiP leader—secretion)	No secretion (Ni-nitrilotriacetic acid purification, small scale, 50 mL)
pMTH (variant of pMT-BiP-V5-HisB)	IL-24wt (52-206)	IL-24-C-His	<i>Drosophila</i> S2 cells (BiP leader—secretion)	No secretion (Ni-nitrilotriacetic acid purification, small scale, 50 mL)
pMTH (variant of pMT-BiP-V5-HisB)	IL-24wt (52-206)	IL-24-C-His	<i>Drosophila</i> S2 cells	No (Ni-nitrilotriacetic acid purification, small scale, 50 mL)
pMTH (variant of pMT-BiP-V5-HisB)	IL-24wt (53-206)	IL-24-C-His	<i>Drosophila</i> S2 cells (BiP leader—secretion)	No secretion (Ni-nitrilotriacetic acid purification, small scale, 50 mL)
pMTH (variant of pMT-BiP-V5-HisB)	IL-24wt (54-206)	IL-24-C-His	<i>Drosophila</i> S2 cells (BiP leader—secretion)	No secretion (Ni-nitrilotriacetic acid purification, small scale, 50 mL)
pMTH (variant of pMT-BiP-V5-HisB)	IL-24short (59-206)	IL-24-C-His	<i>Drosophila</i> S2 cells (BiP leader—secretion)	No secretion (Ni-nitrilotriacetic acid purification, small scale, 50 mL)
pMTH (variant of pMT-BiP-V5-HisB)	IL-24wt (52-206)	IL-24 F109C	<i>Drosophila</i> S2 cells (BiP leader—secretion)	No secretion (Ni-nitrilotriacetic acid purification, small scale, 50 mL)
pMTH (variant of pMT-BiP-V5-HisB)	IL-24wt (52-206)	IL-24 F109C+S101C	<i>Drosophila</i> S2 cells (BiP leader—secretion)	No secretion (Ni-nitrilotriacetic acid purification, small scale, 50 mL)
pMTH (variant of pMT-BiP-V5-HisB)	IL-24 <i>Rattus norvegicus</i> (29-183)	IL-24-C-His	<i>Drosophila</i> S2 cells (BiP leader—secretion)	low yield (western blot)
pMTH (variant of pMT-BiP-V5-HisB)	IL-24 <i>Propithecus coquereli</i>	IL-24-C-His	<i>Drosophila</i> S2 cells	No secretion (Ni-nitrilotriacetic acid purification, small scale, 50 mL)
pMTH (variant of pMT-BiP-V5-HisB)	IL-24 <i>Camelus dromedarius</i>	IL-24-C-His	<i>Drosophila</i> S2 cells	No secretion (Ni-nitrilotriacetic acid purification, small scale, 50 mL)
pMTH (variant of pMT-BiP-V5-HisB)	IL-24wt (52-206) + IL-20R1 (30-250)	IL-24-C-His + IL-20R1-C-His	<i>Drosophila</i> S2 cells (BiP leader—secretion)	No secretion (Ni-nitrilotriacetic acid purification, small scale, 50 mL)

Table 1. (Continued).

Vectors	Insert/Gene	Construct	Organisms/strains tested for expression	Expression
pMTH (variant of pMT-BiP-V5-HisB)	IL-24wt (52-206) + IL-22R1 (22-263)	IL-24-C-His + IL-22R1-C-His	Drosophila S2 cells (BiP leader—secretion)	No secretion (Ni-nitrilotriacetic acid purification, small scale, 50 mL)
pHL-sec-IL-24	IL-24wt (52-206)	IL-24-N-His	HEK293	low yield (western blot)
pcdna3.1	IL-24wt (52-206)	IL-24-N-His	HEK293	low yield (western blot)

relative to human wild-type (Q13007), including four residues (Fig. 3) which were reverted to the wild-type sequence based on analysis of the interface between the IL-20 and IL-20R2 [31]. The IL-24B structure was solved to 1.3 Å resolution by the molecular replacement method and deposited to PDB as 6GG1 (Table 4 and Fig. 3).

Superposition of IL-24B (6GG1) over IL-24L (6DF3, Fig. 4) reveals that 12 of the 34 mutations of IL-24P7 are located at the interfaces with the receptors (Fig. 3, positions 77, 88, 89, 93, 94, 118, 131, 145, 146, 148, 149, and 198). Seven IL-24P7 stabilizing mutations at the positions 88, 89, 145, 146, 148, 149, and 198 could interfere with the receptor binding by their charge and/or volume. To test this possibility, we prepared a set of variants with PROSS mutations changed back to the wild-type residues (designated varA for mutations at the interface with signaling receptors and varB for mutations at the interface with shared receptor IL-20R2, Table 2). The destabilizing effect of the wild-type residues did not allow simultaneous reintroduction of all seven residues (varAB). Reverting the residues 88, 89, and 198 on the interface with signaling receptors 1 caused a substantial decrease in stability so that all three could not be reintroduced simultaneously; even to the most stable variant, IL-24P7, the variant IL-24A was insoluble. Reintroduction of the wild-type residue to the position 89 alone caused a significant decrease in T_m by about 10 °C (varB2). The stability data are corroborated by structural evidence. The mutation R198T in varB4 stabilizes the IL-24B structure by pairing with D194 on the same α -helix, but the bulky positively charged side chain of arginine 198 is approximately in the center of signaling receptors 1 binding interface (Fig. 4B) and it likely obstructs their binding. The reverting of R198T was accompanied with an increase in affinity to IL-22R1 and also the increase in ability to activate STAT3. The increase in affinity and signaling ability is accompanied by a decrease in the thermal stability by 9 °C relative to IL-24P7 but the melting temperature of 74 °C and high yield still makes the IL-24B4 variant useful.

Destabilization is significant but less pronounced for residues at the IL-20R2 interface

We were able to revert four IL-24P7 residues from the interface with IL-20R2 back to the wild-type residues (V145L, L146Q, V148R, and S149K). The resulting IL-24B variant had a lower T_m by 9 °C compared to IL-24P7, and a similar affinity to IL-20R2 as IL-24wt. The presence of charged or bulky amino acids such as Q, R, or K in the above variants is characteristic for the IL-20 sequences at the interface with IL-20R2 where they apparently do not interfere with binding. These residues emerged in PROSS calculations due to the default alignment setting which incorporated also IL-20 orthologs in the calculated multiple sequence alignment. Four other mutated IL-24B residues, E68, R77, R93, D118 from the IL-20R2 interface also occur at the IL-20 interface with IL-20R2 (PDB ID 4DOH [31]). They likely contribute to the binding affinity between the cytokine, IL-20 or IL-24, and shared receptor IL-20R2, as can be seen from high affinities between IL-20R2 and IL-24 variants (Table 2).

The IL-24B structure is a hybrid between the IL-24L and IL-20 structures

Overall, the N-terminal portion of IL-24B structure is more similar to IL-24L and the C-terminal to IL-20 (Fig. 4C). The RMSD diagram reveals that the largest structural differences can be attributed to different S-S bond patterns in IL-24B, IL-24L, and IL-20 (Fig. 2). At the interface with signaling receptors 1 (approximately between residues 70 and 95), the differences between IL-24B and the other two structures are most pronounced, with IL-24B having residues 80–90 missing in the electron density (Fig. 4B). Significantly, the similarity of IL-24B and IL-20 structures between residues 120 and 200 can be explained by a few residues introduced to IL-24B from IL-20 orthologs. Also the binding affinities of IL-24B can be seen as mixing features of IL-24wt and IL-20: while IL-24wt preferentially forms a type II ternary complex, IL-24B type I,

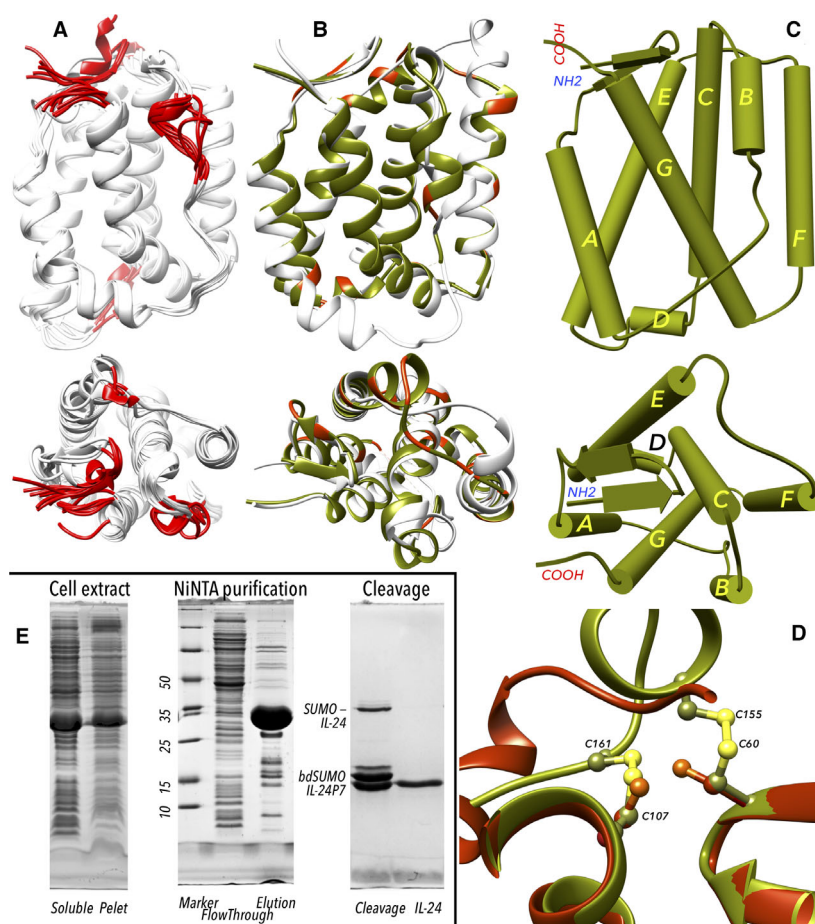


Fig. 2. The design of the IL-24 variants, the structure of IL-24B (PDB ID 6GG1), and representative results of purification. Mutations in IL-24B and other studied variants are listed in Table 2 and highlighted in Fig. 3. (A) The superposition of 10 homologous models used to build the IL-24 homologous model. The highly variable regions (RMSD values > 1 Å) are highlighted in red. (B) The superimposition of 6GG1 (green, mutations from the wild-type in red) over IL-24L (chain C of the IL-24 ternary complex 6DF3, white) [53]. (C) The crystal structure of IL-24B 6GG1 drawn as planks and pipes. The α -helices are labeled A–G. (D) Comparison of the S–S bond patterns in IL-24B (green, 6GG1, cysteine residues labeled), and the unpaired cysteines C8 and C55 from the structure IL-24L (6DF3, red [53]). (E) The representative SDS/PAGE electrophoresis of IL-24P7 purification process. In the first step, the cells were disrupted by sonication and the soluble part was separated by centrifugation (left). The soluble fraction was purified by Ni-nitrilotriacetic acid (middle); shown is flow through and elution in the pooled sample control. The elution fraction was desalted and treated with his-bdSUMO protease (cleavage) over night at room temperature. His-tagged proteins (bdSUMO and his-bdSUMO protease) were removed by additional Ni-nitrilotriacetic acid chromatography and the pure IL-24 protein was collected in flow through. The final purification step was performed by a HiLoad 16/600 Superdex 75.

resembling thus IL-20 (Fig. 1). It is revealing how incorporation of a few mutations can alter the receptor preferences.

Flexibility and promiscuity

The IL-24 and the closely related IL-20 bind to the same two signaling receptors, IL-20R1 and IL-22R1, to form the ternary complexes. The receptors are bound to the same interleukin interfaces, so the interleukin molecules need to be able to accommodate two different binding partners in this region (amino acid

residues 77 and 106 in IL-24 numbering). The expected structural variability in this interface region is confirmed by comparing the structures and sequences of interleukins from the IL-20 family:

- (a) The region between residues 77 and 91 (IL-24 numbering) adopts different structures in free interleukins IL-19 (1N1F [54]), IL-22 (1YKB [55]) and IL-24B (6GG1). However, in complex with the cognate receptors, the region adopts virtually identical structure in IL-24L (6DF3 [53]), IL-20 (4DOH [31]), and IL-22 (3DLQ [56]) including the interacting side chains of signaling receptors 1.

Table 2. Characterization of the IL-24 variants. The mutations in the IL-24P3, P5, and P7 are PROSS-designed variants, IL-24B is the variant that was crystallized and deposited to PDB as 6GG1, IL-24B4 is the variant with restored affinity to the signaling receptors 1 by removing the mutated arginine 198 to the wild-type threonine. The ability to induce STAT3 activation was measured by Signal STAT3 Reporter (luc) Kit on Hela cells and compared to IL-24 wild-type. (A) Wild-type IL-24 and PROSS-designed IL-24 variants. (B) Reverse engineered IL-24 variants. In the Var B variants, we reverted residues at the interface with IL-20R2, in Var A, at the interfaces with the receptors 1 (IL-20R1, IL-22R1).

Protein	Number of mutations	Level of expression	Melting [°C]	Affinity Kd [nM]			STAT3 activity [%]
				IL-20R1	IL-22R1	IL-20R2	
(A)							
IL-24wt ^a	0	No soluble expression BL21 (DE3), low yield HEK293 ≤1 mg·L ⁻¹	59	585	96	469	100
IL-24P3 ^b	5	low yield BL21 (DE3), ≤1 mg·L ^{-1e}	NM				NM
IL-24P5 ^c	16	low yield BL21 (DE3), ≤3 mg·L ^{-1e}	NM				NM
IL-24P7 ^d	34	high yield BL21 (DE3), up to 100 mg·L ⁻¹	83	~ 1500	~ 5000	685	≤5
Protein	Reverted mutations: Mutations removed relative to IL-24P7	Melting [°C]	Affinity Kd [nM]			STAT3 activity [%]	
			IL-20R1	IL-22R1	IL-20R2		
(B)							
IL-24B	V145L, L146Q, V148R, S149K	74	~ 1500	~ 5000	350	< 5	
Var B1	V145L, L146Q, V148R, S149K, S88D	74					
Var B2	V145L, L146Q, V148R, S149K, A89V	67					
Var B3	V145L, L146Q, V148R, S149K, S88D, A89V	67	440	3920	354	≤ 50	
Var B4	V145L, L146Q, V148R, S149K, T198R	74	559	1130	328	80 ± 5	
Var A	S88D, A89V, T198R	Insoluble					
Var AB	V145L, L146Q, V148R, S149K, S88D, A89V, T198R	Insoluble					

NM = Could not be measured.

^aIL-24wt (UniProt ID Q13007 51-206) manufactured by ReproKine (USA) in HEK293 cells with C-terminal His-tag.

^bMutations of IL-24P3: A89T, Q93R, S154C, F160C, I162S.

^cMutations of IL-24P5: S88D, A89V, Q93R, Y107C, R127K, V131L, V148R, S149K, S154C, F160C, I162C, D164E, L172Q, L186A, V193I, K205Q.

^dMutations of IL-24P7: Q60R, K62E, K68E, K77R, M80L, S88D, A89V, Q93R, Q94A, T111Q, E114R, K118D, R127K, V129A, V131L, V145L, L146Q, V148R, S149K, Q150D, S154C, N157Q, E158N, F160C, I162S, D164E, S165E, L172Q, R174Q, K178E, L186A, V193I, T198R, K205Q.

^eUnstable IL-24 variants; the rapid aggregation was observed during purification process.

(b) Superposition of the structures of IL-24L (6DF3) and IL-20 (4DOH) reveals the conserved hydrophobic pocket formed between interleukin helices C, E and F (Figs 2 and 4). We confirmed the importance of this pocket by phylogenetic analysis with two characteristic central residues being, in most cases, two consecutive leucine residues (L91, L92). The hydrophobic pocket and its two central residues orient the part of the structure between R77 and C106, which are responsible for interaction with either receptor 1. The PROSS stabilization altered the position of the conserved leucine residues L91, L92; the shift of the corresponding C alpha atoms between IL-24B and IL-24L is about 0.5 Å. The shift was caused by mutations in the IL-24 inner core, which was made more hydrophobic (Q94A, A134L) and compact (R93Q, Q172L), and despite its relatively small size, it is responsible for lowering the IL-24B affinity to signaling receptors 1.

(c) The residues 93–101 form a highly variable structure among studied cytokines. In IL-24B, this segment is apparently stabilized by contacts formed by mutated residues, for example, R93–E95, creating thus the longest helix in the IL-20 subfamily. The helix side chains, however, retain a substantial flexibility as reflected by multiple rotamer positions identified in the electron density map for residues along the helix (R170, K203, V97).

(d) Side chains of the residues W74, K135, and H125 in IL-24B can be energy minimized to rotameric positions they acquire in IL-24L where they interact attractively with IL-22R1.

Conclusions

We show that an evolutionarily guided, and force-field supported, prediction of stabilizing mutations such as one implemented in the PROSS server [14] is robust enough to be based on homologous models. We

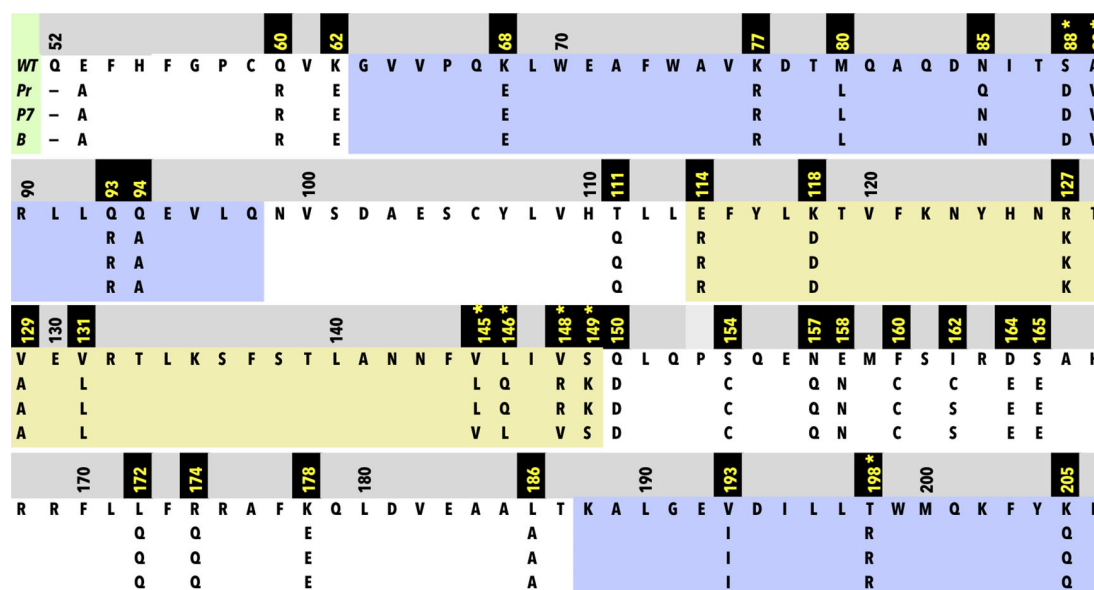


Fig. 3. Multiple sequence alignment of IL-24 sequences. WT (wild-type) sequence corresponds to UniProt ID Q13007, Pr is the PROSS output sequence, P7 (IL-24P7) is sequence of the manually modified version of the Pr sequence as described in the methods, B (IL-24B) is the sequence of IL-24P7 including four residues mutated back to wild-type. The mutations in IL-24P7 compared to UniProt ID Q13007 are labeled as black block above the sequence. The IL-24 residues at the interfaces with the receptors are marked by blue background (receptors 1) and yellow (receptor 2). Seven positions highlighted by stars were identified as potentially interfering with binding and were studied in detail.

generated multiple homology models based on a combination of algorithms, averaged them, and rejected divergent areas. Special care was paid to glycosylation sites, potential S-S bonds, proline conformation, and surface patches known to interact with the receptors molecules.

Our approach can complement experimental methods for protein engineering and represents a viable alternative to research of difficult proteins [40]. It potentially opens up a way to deal with human drug targets for which only *in silico* structural information is available. Such targets are estimated to represent about 40% of all important drug targets. The engineered variants can give us independent structural information and speed up the process of drug screening. The engineered stabilized variants can avoid the need to coexpress with the interaction partners, which may complicate their use for further biological studies.

The designed IL-24 variants can be produced cheaply in large quantities to be used for biochemical studies and further modified to be developed for biomedical applications. The findings are schematically summarized in Fig. 4.

Manual inspection of output from the PROSS server led to the correction of two mutations, one preserving potential glycosylation site, and the other removing an odd cysteine (Fig. 3). The resulting variant IL-24P7 had 34 mutations, almost a quarter of

the IL-24 residues. It was expressed in *E. coli* at very high yields of up to 100 mg·L⁻¹ and was stabilized by 24 °C compared to the wild-type IL-24 (Table 2). We used IL-24P7 as an initial model for studying the role of the mutated amino acid residues to examine protein stability, flexibility, and binding to cognate receptors. The crystal structure of one of them, called IL-24B, was solved at 1.3 Å resolution and deposited to PDB under the code 6GG1. The structural comparison of this apo stabilized construct IL-24B with IL-24L from the ternary complex (6DF3 [53]) confirmed not just the same fold, but overall structural similarity; the RMSD between the corresponding Cα atoms is 1.8 Å. Large structural changes appeared at the interface with signaling receptors 1 (IL-20R1, IL-22R1). We identified residues that interfered with the receptor binding, mutated them back to the wild-type residues, and observed strong negative correlation between the IL-24 stability and its affinity to the signaling receptors 1 (Table 2, Fig. 4). The stabilizing effect of mutated residues is so large that reverting more than a few of them to the wild-type protein resulted in expression of the variants in inclusion bodies. PROSS-designed IL-24P7 contains 34 mutations, six of them in the region interacting with receptors 1 and an additional 5 in close proximity. Reintroduction of just one critical residue to its wild-type (T198R) led to

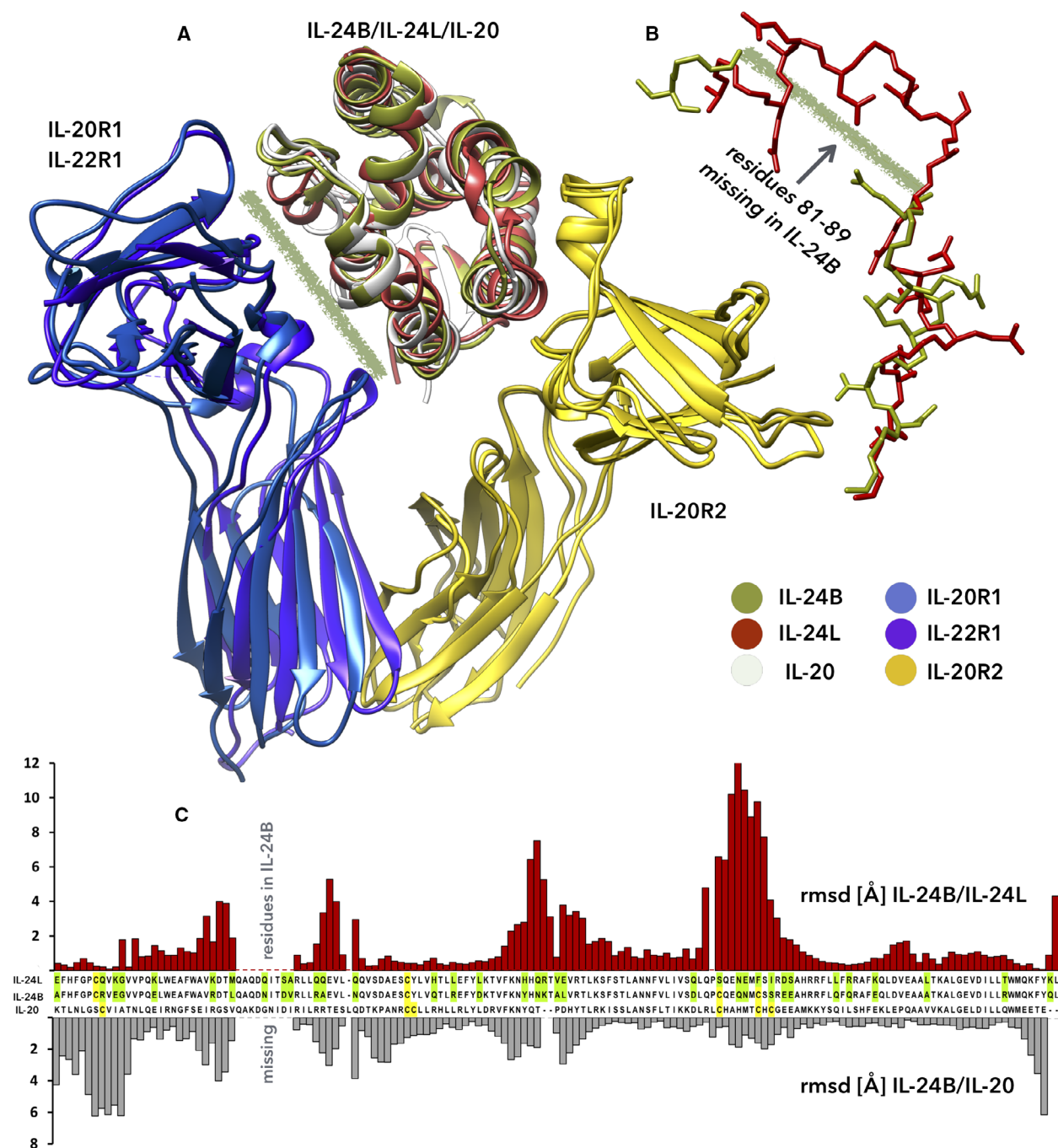


Fig. 4. The comparison of the crystal structures of interleukins IL-24B (in green, 6GG1), IL-24L (in red, 6DF3 [53]), and IL-20 (in white, 4DOH [31]). (A) The superposition of apo IL-24B, and complexes of IL-24L, and IL-20. (B) The blow up highlighting the regions where IL-24B and IL-24L structures differ most. The blurry line highlights the missing residues in the electron density of IL-24B. (C) The diagram displays the RMSD values between the corresponding C α pairs of IL-24B and IL-24L (upper histogram, in red, the average RMSD is 1.8 Å), and IL-24B and IL-20 (lower histogram, in gray, the average 1.4 Å).

restoration of the receptors 1 binding. The IL-24 interface, interacting alternatively with either of the receptors 1, needs to be able to undergo complex structural changes. Experimental mutation analysis

showed that this part of the molecule is crucial for keeping the balance between the stability, and ability to bind to signaling receptors 1 with biologically relevant affinity.

In contrast, the structure at the binding interface of IL-20R2, the shared receptor, was almost unchanged, some residues just adopted different rotamer orientations. The affinity measurements determined a similar affinity between IL-20R2 and IL-24wt, IL-24B, or IL-24P7, so that the residues mutated at this interface did not influence the binding affinity. In addition, they are not critical for the IL-24 stability because we successfully produced a soluble variant with four wild-type residues reintroduced at this interface, albeit accompanied by a loss of 9 °C of the thermal stability (Table 2).

The need for stabilization by interaction with the cognate receptors is characteristic of IL-24 and not observed in the other IL-20 subfamily interleukins. We hypothesize that this inherent instability of IL-24 is the reason for its local action. The IL-24 stability was significantly increased by combination of phylogenetic study, stability calculations, and experiments. The interplay between affinity and stability teaches a lesson for further protein engineering studies: regions with the highest density of suggested mutations are likely important for stability, but they may also be critical for the functioning. As we demonstrated, reverse engineering of these positions could lead to a variant with most of its binding capacity restored, yet stable enough to become an interesting target for biomedical applications.

Methods

Biological material and reagents

Human HeLa cell line was kindly provided by Dr. Cyril Barinka (Institute of Biotechnology, Prague). The cells were maintained in DMEM medium (Thermo Fisher Scientific, Waltham, MA, USA) and regularly subcultured according to the ATCC culturing method (cat. CCL-2™). The *Drosophila melanogaster* Schneider S2 cells were cultivated in the HyClone™ SFX Insect™ (GE Healthcare, Chicago, IL, USA) supplemented with 10% FBS or without sera for expression experiments. Cell suspensions in shaken Erlenmeyer flasks (100 rpm) were incubated at 27 °C. Commercial proteins used in this study were supplied by ReproKine (Tampa, FL, USA) (IL-24wt); PeproTech (Rocky Hill, NJ, USA) (IL-24wt) and by AcroBiosystems (Newark, DE, USA) (IL-20R2). If not stated otherwise, all chemicals and media components were purchased from Merck (Sigma-Aldrich, St. Louis, MO, USA).

Homologous structure-based design of stabilized IL-24

We choose a bioinformatics-based approach to produce IL-24 in amounts suitable for structural biology and biophysical

characterization because numerous previous attempts to express IL-24 were unsuccessful or led to extremely low yields and low protein quality. Initially, comparison of the IL-24 sequence with sequences of the other interleukins of the IL-20 subfamily revealed 34% identity with IL-20 and 29 % identity with IL-19, the values acceptable for homologous modeling [57]. We used IL-19 (PDB: 1N1F, [54]) and IL-20 (PDB: 4DOH, [31]) crystal structures to generate 30 homologous models of IL-24 by using pipelines available in Swiss-model [47], Modeller implemented in Chimera [48,49], and I-TASSER server [50]. Validation of models was performed by SAVES server [58,59]. Models were structurally aligned by Structure Comparison tools and structural comparisons and root-mean-square deviation (RMSD) values were calculated by MatchMaker as implemented in the UCSF Chimera software with the Needleman–Wunsch algorithm and BLOSUM62 matrix. The final structure with overall RMSD value below 1 Å was used for mutation design. The superposition of the models (Fig. 2) showed a high degree of similarity with a few limited regions that required special attention. Particularly, the N-terminal regions differed because of the large differences between the IL-19 and IL-20 structures in this region and these regions were deemed less important in our search for beneficial mutations of more stable IL-24 variants. We randomly selected two models, one based on the IL-19 structure, and the other on the IL-20 structure, and employed the automated design as implemented in the PROSS server [14]. The PROSS-designed mutations largely agreed with those suggested by the FireProt web server [15] but only in cases when the suggestion was based on evolutionary information; no mutations proposed solely by FireProt were incorporated.

Because IL-24 is a secreted protein we paid special attention to the topology of S-S bonds and putative glycosylation sites. PROSS suggested introduction of three cysteine residues, potentially leading to new S-S bonds. Introduction of cysteines seen in IL-20 and IL-19 but not in IL-24 were found as energetically favorable and not in conflict with the calculated homologous models. We decided to include two of these S-S bonds in our design and also test their impact on the wild-type protein (Fig. 2D). Both cysteine residues forming one of the S-S bonds in IL-24B (positions 109–162) were suggested by PROSS; the suggested mutation I162C was changed into I162S.

Although the expression was performed in *E. coli*, we aimed to compare expressions of our constructs also in eukaryotic systems. Therefore, we decided not to include the energetically favored PROSS-designed mutation N85Q in our constructs.

Cloning, mutagenesis, and construction of the expression system

Expression of the different IL-24 variants was performed using the expression vector pET28-bdSumo. This vector was

Project	Primer name	Primer sequence (5' to 3')	
pET28-bdSumo	28_bdSumo_F	TTTGTGTTTAACCTTTAAGAAGGAGATATACCATGAGCAAGCATCACCATCATTCAGG	
	28_bdSumo_R	GGTGGTGGTGCTCGAGTGCGGCCGCAAGCTTGCCACCAGTCTGATGAAGCATTGC	
IL-24 cloning	28Sumo_IL-24_WT_F	ATCGACGCAATGCTTCATCAGACTGGTGGCGCGTTTCATTTTCGGGCCATGCC	
	28Sumo_IL-24_WT_R	GATCTCAGTGGTGGTGGTGGTGGTGCTCGAGTTACAGTTTGTAGAATTTCTGCATCCAGC	
	28Sumo_IL-24_Pross5_F	ATCGACGCAATGCTTCATCAGACTGGTGGCGCGTTCCATTTTCGGTCCTTGTC	
	28Sumo_IL-24_Pross5_R	GATCTCAGTGGTGGTGGTGGTGGTGCTCGAGTTAAAGCTGATAAAACTTTTGCATCCAGG	
	28Sumo_IL-24_Pross7_F	ATCGACGCAATGCTTCATCAGACTGGTGGCGCGTTCCATTTTGGTCCATGTCGTG	
	28Sumo_IL-24_Pross7_R	GATCTCAGTGGTGGTGGTGGTGGTGCTCGAGTTACAGTTGATAAAACTTTTGCATCCAGCG	
Project	Primer name	Variant	Primer sequence (5' to 3')
IL-24 mutagenesis	IL-24P7_4mut_R	varB, VarB1, varB2, varB3, varB4, varAB	CATATTTTGTTCCTGACACGGTTGCAGATCGCTCAGGATCAGCAC GAAATTATTCGCCAGTGTTGAAAAAC
	IL-24P7_2mut_F	varA, varB3varAB	CAAGCTCAGGACAACATCACCAGCGCGCGTTTACTTCGTGCAGA GGTTTTAC
	IL-24P7_R198T_R	varA, varB4varA, varAB	GTTGATAAAACTTTTGCATCCAGGTAAGAAGGATGTCGATCTCTCCC
	IL-24P7_D88S_F	varB1	CAAGCTCAGGACAACATCACCAGCGTACGTTTACTTCGTGCAGAGG
	IL-24P7_V89A_F	varB2	CAAGCTCAGGACAACATCACCAGTACGCGGTTTACTTCGTGCAGAGG
	T7	varB	ATTAATACGACTCACTATAGGGG
	IL-24P7_7mut_R	varAB	CAGTCTTTAAAAACTATCACAATAAGACCG
	IL-24P7_7mut_F	varAB	CACGCGATGAGCACATATTTTGTTC

M9 salts; pH 7.0) supplemented by trace elements TE [64] in 1-L Erlenmeyer flasks with 200 mL of TBTE medium in Max Q 4000 shaker, Barnstead, Lab-Line (250 rpm, 30 °C). Heterologous expression was induced by 1 mM IPTG at OD600 of 0.6, the expression temperature was lowered to 16 °C and growth continued for 16 h. Cells were harvested by centrifugation (5000 *g*, 10 min, 4 °C) and stored in -20 °C for further use.

Cells were disintegrated by sonication (Sonicator 3000, Mixonix, 15-20W) in buffer, (Tris-HCl buffer, pH 8) treated with 5 U·mL⁻¹ Benzonase® Nuclease, centrifuged (40 000 g, 4 °C, 30 min), and loaded on an IMAC HP column charged with NiSO₄ and equilibrated with EQ buffer (50 mM Tris-HCl pH 8, 100 mM NaCl). The column was washed with W buffer (50 mM Tris-HCl, 100 mM NaCl, 20 mM imidazole, pH 8) and the protein was eluted with EL buffer (50 mM Tris-HCl, 100 mM NaCl, 250 mM imidazole, pH 8). The eluted fractions were pooled and further purified with Mini Bio-Gel® P-6 Desalting column (10 mL, equilibrated by EQ buffer) and treated with his-bdSUMO protease (1 : 200, [51,52]) over night at room temperature. His-bdSUMO protease and bdSUMO tag were separated on HisPur™ Ni-nitrilotriacetic acid Resin (Thermo Scientific™) performed as a gravity flow at room temperature. Pure protein was collected as flow through and immediately loaded on a HiLoad 16/600 Superdex 75 gel chromatography column pre-equilibrated in Hepes buffer (50 mM HEPES pH 7.5, 100 mM NaCl) on NGC Chromatography system (Bio-Rad, Hercules, CA).

The cultures of *E. coli* BL21(DE3) were grown in TBs medium (tryptone, 1.2%, yeast extract, 2.4%, glycerol, 0.5%, 1×

USA). The representative SDS/PAGE from purification process is shown in Fig. 2. Identities of all expressed proteins were verified by mass spectrometry.

Expression and purification of recombinant receptor proteins

The extracellular parts of IL-20R1 (UniProt ID Q9UHF4, AA 30–250) and IL-22R1 (UniProt ID Q8N6P7, AA 16 – 228) were produced by the *Drosophila* S2 expression system. The gene sequences were acquired from the NCBI GenBank, optimized for the *Drosophila* codons by the Life Technologies GeneArt Strings Assistant and obtained as DNA Strings. The Strings were cloned into a pMT-BiP-V5-His_A vector (ThermoFisher) using restriction free cloning [63,65] in the position *Bgl*II and *Xho*I restriction sites. It puts both genes in frame with the BiP signal peptide and C-terminal 6x His-Tag. Plasmids were purified by Plasmid Plus Midi Kit (Qiagen, Hilden, Germany) and subsequently *Drosophila* Schneider S2 cells were transfected by using Effectene Transfection Reagent (Qiagen) according to the manufacturer's instructions together with selection plasmid pCoBlast. Stable cell lines were established with 25 µg·mL⁻¹ Blasticidin S. Protein expressions were induced by addition of 1.0 mM CuSO₄. The cell-free media were precipitated by the method described previously [64]. Proteins were purified by HisTrap HP 5 mL (GE Healthcare) columns and HiLoad 16/600 Superdex 75 (GE Healthcare) equilibrated by PBS.

Biological and biophysical characterization

The protein melting curves were acquired by using Prometheus NT.48 (NanoTemper Technologies, Munich, Germany). The instrument detects the change in the tryptophan fluorescence at 330 and 350 nm between 20 °C and 98 °C with 1 °C·min⁻¹ steps and 1 mg·mL⁻¹ of protein. All measurements were done in triplicate. Circular dichroism spectra (CD) were recorded on the Chirascan-plus spectrometer (Applied Photophysics, Beverly, MA, USA) with wavelength steps of 1 nm (185–260 nm) at 25 °C. Protein concentrations were between 0.1 and 0.3 mg·mL⁻¹. The buffer spectra were subtracted and results were analyzed by the CDNN software [66].

IL-24 S-S bond formation was determined by MALDI-MS according to the previously published methods [67,68]. Protein samples were cleaved by trypsin in solution or in 12% SDS/PAGE.

The signaling of engineered variants of IL-24 as well as wild-type proteins was monitored by Signal STAT3 Reporter (luc) Kit according to manufacturer's protocol. Briefly, 5 × 10³ HeLa cells were seeded into 96-well plates BD Falcon 96-well cell culture plate, incubated overnight, and subsequently transfected by the Effectene transfection reagent (Qiagen). After 4 h of incubation, the medium was replaced and cells were recovered for 8 h. Subsequently the media

was supplemented with 100 nM of assayed protein. After 24 h the cells were washed once with ice-cold PBS incubated with 0.25% (w/v) Trypsin 0.53 mM EDTA solution and transferred into Corning® 96 Well White Polystyrene Microplates. The dual-luciferase signal was recorded on a Clariostar Plus microplate reader (BMG Labtech, Ortenberg, Germany) with a Dual-Glo® Luciferase assay system (Promega, Madison, WI, USA).

Affinity measurements

The dissociation constant determination was performed by MicroScale Thermophoresis (MST) using a Monolith NT.115 instrument by NanoTemper Technologies. The receptors IL-20R1 and IL-22R1 were labeled by the Monolith His-Tag Labeling Kit RED-tris-nitrilotriacetic acid and IL-20R2 was labeled by the Monolith NT Protein Labeling Kit (NT-647-NHS) provided by NanoTemper Technologies according to manufacturer's instructions. Labeled proteins were measured in PBS buffer at concentration of 100–200 nM with ranging concentration of a ligand and MST power 20–80%. Data from triplicates were analyzed by the MO. AFFINITY ANALYSIS software version 2.1.2030.

Crystallization

The purified proteins were concentrated by Vivaspin™ protein concentrator spin columns (GE Healthcare) to

Table 4. Data processing statistics and structure refinement parameters of the crystal structure of the IL-24P7 variant, PDB ID 6GG1. Values in parentheses refer to the highest resolution shell

Data processing statistics	
Wavelength (Å)	0.91841
Space group	P2 ₁ 2 ₁ 2 ₁
Unit cell parameters a, b, c (Å)	38.92, 65.37, 67.50
Resolution range (Å)	46.96–1.30 (1.32–1.30)
No. of observations	562 230 (24 971)
No. of unique reflections	43 156 (2091)
Data completeness (%)	100.0 (99.9)
Average redundancy	13.0 (11.9)
Average I/σ(I)	14.7 (1.3)
R _{merge}	0.069 (2.015)
R _{pim}	0.020 (0.631)
CC1/2	0.999 (0.610)
Structure refinement parameters	
R _{work}	0.161
R _{free}	0.183
R _{all}	0.168
Average B-factor (Å ²)	25
RMSD bond lengths from ideal (Å)	0.010
RMSD bond angles from ideal (°)	1.525
Number of nonhydrogen atoms	1468
Number of water molecules	206
Other molecules	2 × SO ₄ ²⁻ , 1 × Ni ²⁺
Ramachandran statistics: residues in favored regions (%)	100

8 mg·mL⁻¹ and directly used for crystallization. Screening experiments were performed with JCSG core suite (Qiagen), Index (Hampton Research, Aliso Viejo, CA, USA), Crystal screen (Hampton Research), Morpheus and Midas (Molecular Dimensions). Diffraction quality crystals were grown using the sitting-drop vapor-diffusion method in 96-3 three-well Intelli-Plate trays (Art Robbins Instruments, Sunnyvale, CA, USA) with the reservoir solution consisting of 20% poly(ethylene glycol) 8000, 0.2 M CaCl₂, 0.1 M MES pH 6. Drops containing 0.2 µL protein sample (8 mg·mL⁻¹ protein) in Hepes buffer and 0.2 µL of reservoir solution were prepared with a Gryphon liquid-pipette robot. After the 4-day growth at ambient temperature (about 293 K), the crystals were mounted in Round LithoLoops (Molecular Dimensions, Maumee, OH, USA) without cryo-protection and flash-cooled in liquid nitrogen.

Data processing, structure determination and refinement

The final diffraction data were collected at the Helmholtz-Zentrum Berlin (BessyII) on a beamline 14.2 equipped Dectris Pilatus 2M detector (Dectris AG, Baden, Switzerland) at 100 K. The diffraction images were processed using XDS [69] and scaled using AIMLESS [70] from the CCP4 program package [71]. The phase problem was solved by molecular replacement using BALBES [72] with the structure of human interleukin-19 (PDB code 1N1F, [54]) as a search model. The structure was refined using REFMAC5 [73] using 95% of reflections as a working set and 5% of reflections as a test set. The last cycle of the refinement was performed using all reflections and anisotropic ADPs for all atoms excluding water molecules. Manual corrections to the model were done using COOT [74]. The structure quality was validated using MOLPROBITY [75]. The atomic coordinates and structure factors were deposited in the Protein Data Bank under the code 6GG1. Data processing statistics and structure refinement parameters are shown in Table 4.

Acknowledgements

This study was supported by the Czech Science Foundation grant 16-20507S and by the projects BIOCEV (CZ.1.05/1.1.00/02.0109), ELIXIR-CZ: building the capacity (CZ.02.1.01/0.0/0.0/16_013/0001777), and CIISB (LM2015043) from the ERDF and MEYS. It was conducted at the Institute of Biotechnology of the Czech Academy of Sciences with the help of the institutional grant RVO 86652036.

Conflict of interest

The authors declare no conflict of interest.

Author Contributions

JZ, LK, BS, and JS planned experiments, analyzed data, and wrote the paper. JZ, LK, YP, PK, SS, TC, and TU performed experiments and analyzed data.

References

- 1 Cohen-Khail R, Dym O, Hamer-Rogotner S & Schreiber G (2017) Promiscuous protein binding as a function of protein stability. *Structure* **25**, 1867–1874.e3.
- 2 Alhindi T, Zhang Z, Ruelens P, Coenen H, Degroote H, Iraci N & Geuten K (2017) Protein interaction evolution from promiscuity to specificity with reduced flexibility in an increasingly complex network. *Scientific Rep* **7**, 44948.
- 3 Garcia-Seisdedos H, Empereur-Mot C, Elad N & Levy ED (2017) Proteins evolve on the edge of supramolecular self-assembly. *Nature* **548**, 244–247.
- 4 Aharoni A, Gaidukov L, Khersonsky O, Mc GS, Roodveldt C & Tawfik DS (2005) The 'evolvability' of promiscuous protein functions. *Nat Genet* **37**, 73–76.
- 5 Magliery TJ (2015) Protein stability: computation, sequence statistics, and new experimental methods. *Curr Opin Struct Biol* **33**, 161–168.
- 6 Wijma HJ, Floor RJ & Janssen DB (2013) Structure- and sequence-analysis inspired engineering of proteins for enhanced thermostability. *Curr Opin Struct Biol* **23**, 588–594.
- 7 Ferdjani S, Ionita M, Roy B, Dion M, Djeghaba Z, Rabiller C & Tellier C (2011) Correlation between thermostability and stability of glycosidases in ionic liquid. *Biotechnol Lett* **33**, 1215–1219.
- 8 Polizzi KM, Bommarius AS, Broering JM & Chaparro-Riggers JF (2007) Stability of biocatalysts. *Curr Opin Struct Biol* **11**, 220–225.
- 9 Fowler DM & Fields S (2014) Deep mutational scanning: a new style of protein science. *Nat Methods* **11**, 801–807.
- 10 Capriotti E, Fariselli P & Casadio R (2005) I-Mutant2.0: predicting stability changes upon mutation from the protein sequence or structure. *Nucleic Acids Res* **33**, W306–W310.
- 11 Borgo B & Havranek JJ (2012) Automated selection of stabilizing mutations in designed and natural proteins. *Proc Natl Acad Sci USA* **109**, 1494–1499.
- 12 Der BS, Kluwe C, Miklos AE, Jacak R, Lyskov S, Gray JJ, Georgiou G, Ellington AD & Kuhlman B (2013) Alternative computational protocols for supercharging protein surfaces for reversible unfolding and retention of stability. *PLoS One* **8**, e64363.
- 13 Jacak R, Leaver-Fay A & Kuhlman B (2012) Computational protein design with explicit consideration of surface hydrophobic patches. *Proteins* **80**, 825–838.

- 14 Goldenzweig A, Goldsmith M, Hill SE, Gertman O, Laurino P, Ashani Y, Dym O, Unger T, Albeck S, Prilusky J, Lieberman RL, Aharoni A, Silman I, Sussman JL, Tawfik DS & Fleishman SJ (2016) Automated structure- and sequence-based design of proteins for high bacterial expression and stability. *Mol Cell* **63**, 337–346.
- 15 Musil M, Stourac J, Bendl J, Brezovsky J, Prokop Z, Zendulka J, Martinek T, Bednar D & Damborsky J (2017) FireProt: web server for automated design of thermostable proteins. *Nucleic Acids Res* **45**, W393–W399.
- 16 Mikulecký P, Černý J, Biedermannová L, Petroková H, Kuchař M, Vondrášek J, Malý P, Šebo P & Schneider B (2013) Increasing affinity of interferon- γ receptor 1 to interferon- γ by computer-aided design. *Biomed Res Int* **2013**, 752514.
- 17 Černý J, Biedermannová L, Mikulecký P, Zahradník J, Charnavets T, Šebo P & Schneider B (2015) Redesigning protein cavities as a strategy for increasing affinity in protein-protein interaction: interferon- γ receptor 1 as a model. *Biomed Res Int* **2015**, 716945.
- 18 Kellogg EH, Leaver-Fay A & Baker D (2011) Role of conformational sampling in computing mutation-induced changes in protein structure and stability. *Proteins* **79**, 830–838.
- 19 Guerois R, Nielsen JE & Serrano L (2002) Predicting changes in the stability of proteins and protein complexes: a study of more than 1000 mutations. *J Mol Biol* **320**, 369–387.
- 20 Jiang H, Lin JJ, Su ZZ, Goldstein NI & Fisher PB (1995) Subtraction hybridization identifies a novel melanoma differentiation associated gene, mda-7, modulated during human melanoma differentiation, growth and progression. *Oncogene* **11**, 2477–2486.
- 21 Soo C, Shaw WW, Freymiller E, Longaker MT, Bertolami CN, Chiu R, Tieu A & Ting K (1999) Cutaneous rat wounds express c49a, a novel gene with homology to the human melanoma differentiation associated gene, mda-7. *J Cell Biochem* **74**, 1–10.
- 22 Zhang R, Tan Z & Liang P (2000) Identification of a novel ligand-receptor pair constitutively activated by ras oncogenes. *J Biol Chem* **275**, 24436–24443.
- 23 Fisher PB (2005) Is mda-7/IL-24 a “Magic Bullet” for cancer? *Cancer Res* **65**, 10128–10138.
- 24 Lebedeva IV, Sauane M, Gopalkrishnan RV, Sarkar D, Su Z, Gupta P, Nemunaitis J, Cunningham C, Yacoub A, Dent P & Fisher PB (2005) mda-7/IL-24: Exploiting cancer’s achilles’ heel. *Mol Therap* **11**, 4–18.
- 25 Kreis S, Philippidou D, Margue C, Rolvering C, Haan C, Dumoutier L, Renauld JC & Behrmann I (2007) Recombinant interleukin-24 lacks apoptosis-inducing properties in melanoma cells. *PLoS One* **2**, e1300.
- 26 Kreis S, Philippidou D, Margue C & Behrmann I (2008) IL-24: a classic cytokine and/or a potential cure for cancer? *J Cell Mol Med* **12**, 2505–2510.
- 27 Dumoutier L, Leemans C, Lejeune D, Kotenko SV & Renauld JC (2001) Cutting edge: STAT activation by IL-19, IL-20 and mda-7 through IL-20 receptor complexes of two types. *J Immunol* **167**, 3545–3549.
- 28 Wang M & Liang P (2005) Interleukin-24 and its receptors. *Immunology* **114**, 166–170.
- 29 Rutz S, Wang X & Ouyang W (2014) The IL-20 subfamily of cytokines—from host defence to tissue homeostasis. *Nat Rev Immunol* **14**, 783–795.
- 30 Pletnev S, Magracheva E, Kozlov S, Tobin G, Kotenko SV, Wlodawer A & Zdanov A (2003) Characterization of the recombinant extracellular domains of human interleukin-20 receptors and their complexes with interleukin-19 and interleukin-20. *Biochemistry* **42**, 12617–12624.
- 31 Logsdon NJ, Deshpande A, Harris BD, Rajashankar KR & Walter MR (2012) Structural basis for receptor sharing and activation by interleukin-20 receptor-2 (IL-20R2) binding cytokines. *Proc Natl Acad Sci USA* **109**, 12704–12709.
- 32 Oral HB, Kotenko SV, Yilmaz M, Mani O, Zumkehr J, Blaser K, Akdis CA & Akdis M (2006) Regulation of T cells and cytokines by the interleukin-10 (IL-10)-family cytokines IL-19, IL-20, IL-22, IL-24 and IL-26. *Eur J Immunol* **36**, 380–388.
- 33 Akdis M, Burgler S, Cramer R, Eiwegger T, Fujita H, Gomez E, Klunker S, Meyer N, O’Mahony L, Palomares O, Rhyner C, Ouaked N, Schaffartzik A, Van De Veen W, Zeller S, Zimmermann M & Akdis CA (2011) Interleukins, from 1 to 37, and interferon-gamma: receptors, functions, and roles in diseases *J Allergy Clin Immunol* **127**, 701–21.e1–70.
- 34 Kumari S, Bonnet MC, Ulmar MH, Wolk K, Karagianni N, Witte E, Uthoff-Hachenberg C, Renauld JC, Kollias G, Toftgard R, Sabat R, Pasparakis M & Haase I (2013) Tumor necrosis factor receptor signaling in keratinocytes triggers interleukin-24-dependent psoriasis-like skin inflammation in mice. *Immunity* **39**, 899–911.
- 35 Jin SH, Choi D, Chun YJ & Noh M (2014) Keratinocyte-derived IL-24 plays a role in the positive feedback regulation of epidermal inflammation in response to environmental and endogenous toxic stressors. *Toxicol Appl Pharmacol* **280**, 199–206.
- 36 Andoh A, Shioya M, Nishida A, Bamba S, Tsujikawa T, Kim-Mitsuyama S & Fujiyama Y (2009) Expression of IL-24, an activator of the JAK1/STAT3/SOCS3 cascade, is enhanced in inflammatory bowel disease. *J Immunol* **183**, 687–695.
- 37 Fonseca-Camarillo G, Furuzawa-Carballeda J, Granados J & Yamamoto-Furusho JK (2014) Expression of interleukin (IL)-19 and IL-24 in

- inflammatory bowel disease patients: a cross-sectional study. *Clin Exp Immunol* **177**, 64–75.
- 38 Ma Y, Chen H, Wang Q, Luo F, Yan J & Zhang XL (2009) IL-24 protects against *Salmonella typhimurium* infection by stimulating early neutrophil Th1 cytokine production, which in turn activates CD8⁺ T cells. *Eur J Immunol* **39**, 3357–3368.
 - 39 Zhang J, Lv X, Xu R, Tao X, Dong Y, Sun A & Wei D (2015) Soluble expression, rapid purification, and characterization of human interleukin-24 (IL-24) using a MBP-SUMO dual fusion system in *Escherichia coli*. *Appl Microbiol Biotechnol* **99**, 6705–6713.
 - 40 Smoddy JC, MacKinnon SS & Windemuth A (2017) Structural coverage of the proteome for pharmaceutical applications. *Drug Discov Today* **22**, 1792–1799.
 - 41 Yang J, Zhang W, Liu K, Jing S, Guo G, Luo P & Zou Q (2007) Expression, purification, and characterization of recombinant human interleukin 24 in *Escherichia coli*. *Protein Expr Purif* **53**, 339–345.
 - 42 Xiao B, Li W, Yang J, Guo G, Mao XH & Zou QM (2009) RGD-IL-24, a novel tumor-targeted fusion cytokine: expression, purification and functional evaluation. *Mol Biotechnol* **41**, 138–144.
 - 43 Xie Y, Sheng W, Xiang J, Ye Z, Zhu Y, Chen X & Yang J (2008) Recombinant human IL-24 suppresses lung carcinoma cell growth via induction of cell apoptosis and inhibition of tumor angiogenesis. *Cancer Biother Radiopharm* **23**, 310–320.
 - 44 Amirzadeh MI, Yu M, Gong X, Chen Y, Zhu R, Lei J & Jin J (2014) Cost-effective production of recombinant human interleukin 24 by lactose induction and a two-step denaturing and one-step refolding method. *J Ind Microbiol Biotechnol* **41**, 135–142.
 - 45 Wang X, Bai C, Zhang J, Sun A, Wang X & Wei D (2014) Improving the mda-7/IL-24 refolding and purification process using optimized culture conditions based on the structure characteristics of inclusion bodies. *Biores Bioprocess* **1**, 21.
 - 46 Traxlmayr MW & Obinger C (2012) Directed evolution of proteins for increased stability and expression using yeast display. *Arch Biochem Biophys* **526**, 174–180.
 - 47 Bordoli L & Schwede T (2012) Automated protein structure modeling with SWISS-MODEL Workspace and the Protein Model Portal. *Methods Mol Biol (Clifton, NJ)* **857**, 107–136.
 - 48 Eswar N, Webb B, Marti-Renom MA, Madhusudhan MS, Eramian D, Shen MY, Pieper U & Sali A (2006) Comparative protein structure modeling using Modeller. *Curr Protoc Bioinformatics* Chapter 5, Unit-5.6.
 - 49 Pettersen EF, Goddard TD, Huang CC, Couch GS, Greenblatt DM, Meng EC & Ferrin TE (2004) UCSF Chimera—a visualization system for exploratory research and analysis. *J Computat Chem* **25**, 1605–1612.
 - 50 Yang J & Zhang Y (2015) Protein Structure and Function Prediction Using I-TASSER. *Curr Protoc Bioinformatics* **52**, 5.8.1–15.
 - 51 Frey S & Gorlich D (2014) A new set of highly efficient, tag-cleaving proteases for purifying recombinant proteins. *J Chrom A* **1337**, 95–105.
 - 52 Frey S & Gorlich D (2014) Purification of protein complexes of defined subunit stoichiometry using a set of orthogonal, tag-cleaving proteases. *J Chrom A* **1337**, 106–115.
 - 53 Lubkowski J, Sonmez C, Smirnov SV, Anishkin A, Kotenko SV & Wlodawer A (2018) Crystal Structure of the Labile Complex of IL-24 with the Extracellular Domains of IL-22R1 and IL-20R2. *J Immunol*, jil800726.
 - 54 Chang C, Magracheva E, Kozlov S, Fong S, Tobin G, Kotenko S, Wlodawer A & Zdanov A (2003) Crystal structure of interleukin-19 defines a new subfamily of helical cytokines. *The J Biol Chem* **278**, 3308–3313.
 - 55 Xu T, Logsdon NJ & Walter MR (2005) Structure of insect-cell-derived IL-22. *Acta Crystallogr D* **61**, 942–950.
 - 56 Bleicher L, de Moura PR, Watanabe L, Colau D, Dumoutier L, Renauld J-C & Polikarpov I (2008) Crystal structure of the IL-22/IL-22R1 complex and its implications for the IL-22 signaling mechanism. *FEBS Lett* **582**, 2985–2992.
 - 57 Xiang Z (2006) Advances in homology protein structure modeling. *Curr Protein Pept Sci* **7**, 217–227.
 - 58 Luthy R, Bowie JU & Eisenberg D (1992) Assessment of protein models with three-dimensional profiles. *Nature* **356**, 83–85.
 - 59 Laskowski RA, MacArthur MW, Moss DS & Thornton JM (1993) PROCHECK: a program to check the stereochemical quality of protein structures. *J Appl Crystallogr* **26**, 283–291.
 - 60 Peleg Y & Unger T (2008) Application of high-throughput methodologies to the expression of recombinant proteins in *E. coli*. *Methods Mol Biol* **426**, 197–208.
 - 61 Erijman A, Dantes A, Bernheim R, Shifman JM & Peleg Y (2011) Transfer-PCR (TPCR): a highway for DNA cloning and protein engineering. *J Struct Biol* **175**, 171–177.
 - 62 Erijman A, Shifman JM & Peleg Y (2014) A single-tube assembly of DNA using the transfer-PCR (TPCR) platform. *Methods Mol Biol* **1116**, 89–101.
 - 63 Peleg Y & Unger T (2014) Application of the Restriction-Free (RF) cloning for multicomponents assembly. *Methods Mol Biol* **1116**, 73–87.
 - 64 Zahradník J, Kolářová L, Pařízková H, Kolenko P & Schneider B (2018) Interferons type II and their receptors R1 and R2 in fish species: Evolution, structure, and function. *Fish Shellfish Immunol* **79**, 140–152.

- 65 Bond SR & Naus CC (2012) RF-Cloning.org: an online tool for the design of restriction-free cloning projects. *Nucleic Acids Res* **40**, W209–W213.
- 66 Bohm G, Muhr R & Jaenicke R (1992) Quantitative analysis of protein far UV circular dichroism spectra by neural networks. *Protein Eng* **5**, 191–195.
- 67 Pompach P, Man P, Kavan D, Hofbauerova K, Kumar V, Bezouska K, Havlicek V & Novak P (2009) Modified electrophoretic and digestion conditions allow a simplified mass spectrometric evaluation of disulfide bonds. *J Mass Spectrom* **44**, 1571–1578.
- 68 Mikulecky P, Zahradník J, Kolenko P, Cerny J, Charnavets T, Kolarova L, Necasova I, Pham PN & Schneider B (2016) Crystal structure of human interferon-gamma receptor 2 reveals the structural basis for receptor specificity. *Acta Crystallogr D* **72**, 1017–1025.
- 69 Kabsch W (2010) XDS. *Acta Crystallogr D Struct Biol* **66**, 125–32.
- 70 Evans PR (2011) An introduction to data reduction: space-group determination, scaling and intensity statistics. *Acta Crystallogr D* **67**, 282–292.
- 71 Winn MD, Ballard CC, Cowtan KD, Dodson EJ, Emsley P, Evans PR, Keegan RM, Krissinel EB, Leslie AG, McCoy A, McNicholas SJ, Murshudov GN, Pannu NS, Potterton EA, Powell HR, Read RJ, Vagin A & Wilson KS (2011) Overview of the CCP4 suite and current developments. *Acta Crystallogr D* **67**, 235–242.
- 72 Long F, Vagin AA, Young P & Murshudov GN (2008) BALBES: a molecular-replacement pipeline. *Acta Crystallogr D* **64**, 125–132.
- 73 Murshudov GN, Skubák P, Lebedev AA, Pannu NS, Steiner RA, Nicholls RA, Winn MD, Long F & Vagin AA (2011) REFMAC5 for the refinement of macromolecular crystal structures. *Acta Crystallogr D* **67**, 355–367.
- 74 Emsley P, Lohkamp B, Scott WG & Cowtan K (2010) Features and development of Coot. *Acta Crystallogr D* **66**, 486–501.
- 75 Chen VB, Arendall WB, Headd JJ, Keedy DA, Immormino RM, Kapral GJ, Murray LW, Richardson JS & Richardson DC (2010) MolProbity: all-atom structure validation for macromolecular crystallography. *Acta Crystallogr D* **66**, 12–21.